QUANTITATIVE ANALYSIS OF Q-SPACE MRI DATA

L.G. Raguin*, D. Hernando**, D. Karampinos*, L. Ciobanu***, B.P. Sutton***, Z.-P. Liang*** and J.G. Georgiadis*

* University of Illinois at Urbana–Champaign, Department of Mechanical & Industrial Engineering, Laboratory of Quantitative Visualization in Energetics, Urbana, IL, USA
** University of Illinois at Urbana–Champaign, Department of Electrical & Computer Engineering, Urbana, IL, USA
*** University of Illinois at Urbana–Champaign, Biomedical Imaging Center, Beckman Institute, Urbana, IL, USA

raguin@uiuc.edu

Abstract:
A quantitative analysis of q-space MRI data (QUAQ) is presented to extract the physical parameters of diffusion in fiber networks and resolve fiber crossings, e.g. for brain white matter fiber tracking. This method is based on the analytical expression for the normalized echo attenuation $E(q)$ in cylindrical pores measured by pulsed-gradient MRI in the short pulse approximation, which reflects the restricted diffusion process inside the fibers. An alternative method (MDTI) consists in approximating $E(q)$ by a sum of Gaussian distributions, which corresponds to the assumption that the diffusion process in the fibers reduces to unrestricted anisotropic diffusion. These two methods are validated and compared both numerically and experimentally, and the influence of the distribution of the input measurements in q-space (number of gradient strengths and orientations) on the results is investigated.

Introduction

In the last decade, diffusion-weighted magnetic resonance imaging (DW-MRI) has been increasingly applied to track fibers in soft biological tissues such as brain white matter non-invasively [1]. DW-MRI produces maps of the echo attenuation that depend on the local diffusion process and are indexed by a value in $\boldsymbol{q}$-space corresponding to the experimental parameters [2]. Different modalities exist to extract valuable information from DW-MRI data: diffusion tensor imaging (DTI) reconstructs the local diffusion tensor [1]; diffusion spectrum imaging (DSI), a.k.a. $\boldsymbol{q}$-space imaging (QSI), extracts the local distribution of the spin displacements, a.k.a. the 3D average propagator, based on the (extensive) sampling of the echo attenuation in $\boldsymbol{q}$-space [3]. The fiber orientation is identified with the direction of maximum diffusion and thus longest displacements. DTI cannot resolve crossing fibers, while DSI is a promising albeit time-consuming method [3]. More complex methods have also been developed recently to elucidate fiber crossings: composite hindered and restricted model of diffusion (CHARMED [4]), q-ball imaging (QBI [5]), and high angular resolution diffusion imaging (HARDI [6]). In the latter, the signal is acquired with high angular resolution in $\boldsymbol{q}$-space and then decomposed into a discrete mixture of Gaussian diffusion processes in slow exchange. This amounts to a multi-modal version of DTI that we call MDTI. In this work, we present an alternative: a quantitative analysis of $\boldsymbol{q}$-space MRI data (QUAQ) that merges $\boldsymbol{q}$-space MRI with the physics of the diffusion process inside a network of cylindrical fibers, and quantitatively estimate the characteristics of the system (diffusion constants and fiber orientations). In addition, we compare the QUAQ method to MDTI both numerically and experimentally by using a synthetic diffusion phantom.

Methodology

Considering a population of spins subjected to a spin-echo (SE) pulse sequence in the presence of two magnetic field gradient pulses ($\boldsymbol{g}$) of duration δ and separation Δ (a.k.a. diffusion time), Tanner and Stejskal [7] showed that the normalized echo attenuation $E(\boldsymbol{q}, \Delta)$ is proportional to the Fourier transform of the average propagator, and $\boldsymbol{q} = \gamma \boldsymbol{g} \delta / 2\pi$ plays the role of a spatial frequency corresponding to the displacement of the spins. In practice, $E(\boldsymbol{q}, \Delta)$ is obtained by dividing the measured echo with diffusion-encoding gradients, $S(\boldsymbol{q}, \Delta)$, by the echo obtained with zero diffusion gradients, $S(\boldsymbol{q} = \mathbf{0}, \Delta)$. The inverse Fourier transform of $E(\boldsymbol{q}, \Delta)$ yields the 3D average propagator, and thus the orientation of the fibers in each voxel can be inferred. However, a large number (~ 500) of orientations and magnitudes of $\boldsymbol{q}$ are needed to reconstruct the 3D propagator [3]. In order to extract the fiber orientation from MRI data, one requirement must be met: the diffusion time experienced by the spins must be large enough so that enough spins reach the fiber boundaries, i.e.

$$\Delta \gtrapprox \frac{a^2}{2D_\perp}, \tag{1}$$

where $D_\perp$ is the diffusion coefficient in the direction transverse to the fiber orientation. If on the contrary $\Delta \ll a^2/2D_\perp$, then the diffusion process can be mod-

ISSN: 1727-1983

eled by unrestricted anisotropic diffusion if the diffusion coefficient parallel to the fiber, $D_{\|}$, is different than $D_{\perp}$, or by isotropic diffusion if $D_{\|} \sim D_{\perp}$.

Let us consider *non-communicating* cylindrical fibers in a *non-participating external medium* (i.e. the medium does not produce any MR signal). In cases where the medium does produce an MR signal, it can be modeled as a hindered compartment following the formulation in [4]. Diffusion inside a single cylindrical fiber with radius a_m oriented along the x-axis for a diffusion time Δ is associated with an *average propagator* $\overline{P}_m(\boldsymbol{x}, \Delta; a_m)$ that is a function of the displacement $\boldsymbol{x}$ and is parameterized by the fiber radius a_m. The average propagator for a fiber in any other orientation in spherical coordinates (θ_m, ψ_m) is then given by $\overline{P}_m(\boldsymbol{R}^{-1}(\theta_m, \psi_m)\boldsymbol{x}, \Delta; a_m)$, where $\boldsymbol{R}(\theta, \psi)$ is the appropriate 3×3 transformation matrix that rotates $\boldsymbol{x}$ into the frame of reference of the fiber.

If each voxel contains a distribution of M crossing fibers with varying radii (a_m, $m \in [1, M]$) and orientations (θ_m, ψ_m), the average propagator $\overline{P}(\boldsymbol{x}, \Delta)$ can be decomposed into

$$\overline{P}(\boldsymbol{x}, \Delta) = \sum_{m=1}^{M} v_m \overline{P}_m(\boldsymbol{R}^{-1}(\theta_m, \psi_m)\boldsymbol{x}, \Delta; a_m), \quad (2)$$

where v_m is the volume fraction of the fibers with orientation (θ_m, ψ_m) and radius a_m. Let

$$E_m(\boldsymbol{q}, \Delta) = \int \overline{P}_m(\boldsymbol{x}, \Delta : a_m) \mathrm{e}^{2\pi \mathrm{i} \boldsymbol{q} \cdot \boldsymbol{x}} \mathrm{d}\boldsymbol{x}. \quad (3)$$

It follows that the normalized echo attenuation can be expressed by

$$E(\boldsymbol{q}, \Delta) = \sum_{m=1}^{n} f_m E_m(\boldsymbol{R}^{-1}(\theta_m, \psi_m)\boldsymbol{q}, \Delta). \quad (4)$$

Note that each f_m is proportional to the volume fraction v_m, but it also depends on the imaging parameters and relaxation times within the fibers with orientation (θ_m, ψ_m) and radius a_m. Therefore, f_m replaces v_m in the echo attenuation expression, and it is termed the signal-weighted volume fraction. Since the echo attenuation is normalized and we have assumed that the signal only comes from the fibers (non-participating medium), we have one additional constraint:

$$\sum_{m=1}^{M} f_m = 1 \quad \text{or} \quad f_M = 1 - \sum_{m=1}^{M-1} f_m. \quad (5)$$

Moreover, it is assumed that the fluid inside all the fibers has the same diffusivities, i.e. $D_{\|}$ and $D_{\perp}$ are independent of m. Extrapolation to the case where the diffusivities do depend on m is trivial, although to identify the additional parameters requires more data input.

Equation (4) can then be interpreted as a projection of the normalized echo attenuation onto a set of basis functions with parameters (θ_m, ψ_m, a_m), and the multiplying coefficients corresponding to the signal-weighted volume fraction f_m of the fibers. This is the rationale behind the QUAQ approach.

Analytical solutions exist for the propagator and the corresponding function $E_m(\boldsymbol{q}, \Delta; a_m)$ in certain configurations [8], from which their Fourier transform can be obtained, and then the basis functions in Eq. (4) become known. A simple but qualitative model would be to assume that the average propagator for a single fiber is described by a Gaussian distribution. This means that diffusion in a single channel can be interpreted as an unrestricted anisotropic diffusion process. Then, the signal expression for a single fiber is also a Gaussian distribution as a function of $\boldsymbol{q}$. This is the assumption on which DTI is based, and the experimental data are used to obtain the "apparent" diffusion tensor. When multiple fibers are assumed to be present in the voxel of interest under the previous assumptions, the normalized echo attenuation becomes a multi-Gaussian decomposition of the MR signal:

$$E(\boldsymbol{q}, \Delta) = \sum_{m=1}^{n} f_m \exp\left[-4\pi^2 \Delta\, \boldsymbol{q}^{\mathrm{T}} \cdot \boldsymbol{D}_m \cdot \boldsymbol{q}\right]. \quad (6)$$

Therefore, the assumption that the propagator for a single fiber is described by a Gaussian distribution reduces ours to the model used for MDTI (and recovers the expression derived in [6]). In the present formulation, the individual apparent diffusion tensors,

$$\boldsymbol{D}_m = \boldsymbol{R}^{\mathrm{T}}(\theta_m, \psi_m)\boldsymbol{D}\boldsymbol{R}(\theta_m, \psi_m), \quad (7)$$

are parameterized by the orientations (θ_m, ψ_m) via the matrix of eigenvectors $\boldsymbol{R}$, and the signal-weighted volume fraction (f_m) of the fibers, where $\boldsymbol{D}$ is a diagonal matrix with eigenvalues $D_{\|}$ along the longitudinal direction of the fiber and $D_{\perp}$ along the transverse direction(s). However, since it is known that the propagator for a single fiber cannot in general be approximated by a Gaussian distribution, a more sophisticated description of the diffusion process is necessary.

Based on the analytical results for cylindrical fibers by Callaghan [8] which assumes short pulsed gradients (duration of gradients $\delta \ll$ diffusion time Δ), an analytical formula is derived for the normalized echo attenuation for a fluid inside M cylindrical fibers of radius a_m ($m \in [1, M]$). To account for the layered structure of the brain white matter fibers, the diffusion process within the fiber is assumed to be anisotropic with parallel diffusivity $D_{\|}$ and transverse diffusivity $D_{\perp}$. For M fibers in an extra-axonal environment that produces no MR signal, the echo attenuation is fitted to Eq. (8), where $\boldsymbol{q}$ is separated into its longitudinal and transverse components ($\boldsymbol{q} = \boldsymbol{q}_{\|} + \boldsymbol{q}_{\perp}$), $q_{\|} = \|\boldsymbol{q}_{\|}\|$, $q_{\perp} = \|\boldsymbol{q}_{\perp}\|$, and $\beta_{n,k}$ is the k^{th} root of the first derivative of the Bessel function of order n, J_n ($J'_n(\beta_{n,k}) = 0$). $E(\boldsymbol{q}, \Delta)$ given by Eq. (8) depends on the experimental parameters (δ, Δ, diffusion gradient $\boldsymbol{g}$) and the physical parameters of the problem ($a_m, D_{\|}, D_{\perp}, \theta_m, \psi_m, f_m$). A Levenberg-Marquardt al-

ISSN: 1727-1983

$$E(\boldsymbol{q},\Delta) = \sum_{m=1}^{M} f_m \left\{ 4\left(\frac{J_0'(2\pi a_m q_\perp)}{2\pi a_m q_\perp}\right)^2 + 4\sum_{k=1}^{\infty}\left(\frac{2\pi a_m q_\perp J_0'(2\pi a_m q_\perp)}{(2\pi a_m q_\perp)^2-\beta_{0,k}^2}\right)^2 \exp\left(-\beta_{0,k}^2\frac{D_\perp}{a_m^2}\Delta\right) + 8\sum_{n=1}^{\infty}\sum_{k=1}^{\infty}\frac{\beta_{n,k}^2}{\beta_{n,k}^2-n^2}\left(\frac{2\pi a_m q_\perp J_n'(2\pi a_m q_\perp)}{(2\pi a_m q_\perp)^2-\beta_{n,k}^2}\right)^2 \exp\left(-\beta_{n,k}^2\frac{D_\perp}{a_m^2}\Delta\right)\right\} \exp\left(-4\pi^2 D_\parallel q_\parallel^2 \Delta\right). \quad (8)$$

gorithm [9] is used to solve the nonlinear least-squares minimization problem of fitting the echo attenuation data to the analytical formula. The fitting parameters are $(D_\parallel, D_\perp, f_m, \theta_m, \psi_m)$, while the fiber sizes a_m are assumed to be known (e.g. via histology). The infinite series in Eq. (8) are truncated, which is allowed since the exponential terms in the series vanish as n and k increase. Note that these terms vanish faster if the diffusion time Δ is large w.r.t. $a^2/D_\perp$, cf. Eq. (1). The level of truncation can be estimated from the assumed a_m value, an estimated $D_\perp$ value and the known value of Δ. This fitting procedure constitutes the QUAQ algorithm to reconstruct the fibers pixel-per-pixel based on $\boldsymbol{q}$-space MRI data.

In a similar approach, Assaf et al. [4] proposed fitting the normalized echo attenuation to a different analytical expression. The direction parallel (subscript $\parallel$) to the cylindrical fiber can be decoupled from the direction transverse (subscript $\perp$) to the fiber, and the echo attenuation takes the form of a product of two echo attenuation components, $E_{m\parallel}$ and $E_{m\perp}$. The expression for $E_{m\parallel}$ corresponds to pulse-field gradient imaging of 1D unrestricted Gaussian diffusion *without* assuming that $\delta \ll \Delta$, which matches the QUAQ approach (8) with an effective diffusion time equal to $\Delta - \delta/3$. The difference lies in the expression for $E_{m\perp}$, which is derived in [10] and requires (i) *steady gradient* SE imaging (i.e. $\delta = \Delta = \tau$, where τ is the echo time of the SE sequence) and (ii) that the diffusion time be long compared to the time necessary for the spins to hit the boundaries, i.e. $\tau \gg a_m^2/D_\perp$. Clearly, the steady gradient assumption employed for $E_{m\perp}$ is not consistent with that of pulsed field gradient SE imaging used both for $E_{m\parallel}$ and for their experiments. Moreover, Assaf et al. [4] assume in practice that the values for the fiber sizes a_m and the transverse diffusivity $D_\perp$ are known *a priori*. Consequently, $E_{m\perp}$ is fully known and their methodology reduces to performing a Gaussian fit of the data. Additionally, while the size of the fibers can be measured by histology, it is more difficult to envision how $D_\perp$ would be measured.

Our proposed method is first tested numerically and compared to MDTI. The influence of the sampling of $\boldsymbol{q}$-space (number of g values and orientations), the presence of noise in the input data, and the possibility of data averaging to reduce the noise level is investigated. The noise is introduced in the synthetic data as rectified Gaussian noise [11]. An experimental validation is also provided to show that the crossing of two fiber bundles can be retrieved in the presence of experimental noise.

Numerical results

Let us consider two cases: one single fiber and crossing fibers with relative angle $46.62°$, with $a_1 = a_2 = 50$ μm and other input parameters in Table 1 and the following experimental parameters: $\delta = 5$ ms, $\Delta = 250$ ms. The series in Eq. (8) are truncated at $n = 3$ and $k = 6$ and the signal is sampled over 100 trials with Rician noise added to give SNR $= 10$ in the non-diffusion-attenuated signal. Typical results are presented in Table 1 where 45 $\boldsymbol{q}$ values are used ($g = 3, 4, 5$ G cm^{-1} and 15 orientations). For the relatively low SNR value we chose (corresponding to a normalized rms difference between the data in $\boldsymbol{q}$-space with and without noise of 3.9%), QUAQ performs well for a limited number of data points (here 45 $\boldsymbol{q}$ values) compared to what is typically used (e.g. 127 for HARDI [6], 253 for QBI [5], 496 for CHARMED [4], and 515 for DSI [3]). The MDTI results are also in good agreement for $D_\parallel$, θ_1 and ψ_1, but $D_\perp$ gets underestimated.

Table 1: Results for a single fiber ($f_1 = 1$) and two crossing fibers ($f_1 = f_2 = 0.5$) using 3 g values and 15 orientations (i.e. 45 $\boldsymbol{q}$ values). The fit error is the normalized rms error between the fit and the noisy input signal, while the absolute error compares the fit and the exact signal

Parameter	**Input**	**Single fiber**		**Crossing fibers**	
		QUAQ	**MDTI**	**QUAQ**	**MDTI**
f_1	1.0 / 0.5	1.0	1.0	0.565	0.591
$D_\parallel \times 10^9$ (m^2 s^{-1})	2.000	1.913	1.918	1.915	1.927
$D_\perp \times 10^9$ (m^2 s^{-1})	2.000	1.929	1.213	1.913	1.204
θ_1 (°)	11.46	12.09	12.09	21.2	22.76
ψ_1 (°)	28.66	29.12	29.18	28.83	30.12
θ_2 (°)	45.86	–	–	48.32	49.12
ψ_2 (°)	68.79	–	–	73.61	75.78
Fit error	–	2.34%	2.42%	2.13%	2.29%
Abs. error	–	2.87%	2.89%	3.20%	3.23%

The results for two crossing fibers are similar: QUAQ extracts all the physical parameters of the problem, albeit with slightly larger errors, and so does MDTI except for $D\perp$ which is again underestimated (Table 1). Figure 1 illustrates the inability of MDTI to capture the correct shape of the signal in $\boldsymbol{q}$-space by showing the contour lines of the echo attenuation based on the correct analytical formula and the contour lines of the multi-Gaussian approximation. The errors on the angles for both methods (up to 10°) are reasonable considering the amount

ISSN: 1727-1983

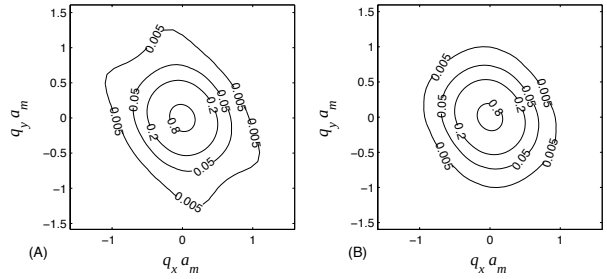

Figure 1: Contour lines of the echo attenuation in the plane of the crossing fibers computed from (A) the QUAQ equation (8), and (B) the MDTI equation (6) for the parameters given in Table 1 and $a_m^2/D_\perp \Delta = 5$

of noise and SNR value. The rms errors remain close to the ones obtained for single fibers because the sensitivity of the signal to the orientations for the chosen q values ($qa_m < 0.55$) is relatively low, cf. Figure 1.

Experimental results

A 2 cm $\times$ 2 cm $\times$ 1 cm phantom was built using two sets of perpendicular crossing PTFE fibers (Cole–Parmer Instrument Company, Vernon Hills, IL, USA) with $a_1 = a_2 = 50$ μm, filled with water ($D_\parallel = D_\perp = 1.6 \times 10^{-9}$ m^2 s^{-1} at 11.5°C [12] and placed in an Varian 14.1 T NMR imager. Copper sulphate was added to the water to decrease the relaxation time T_1, and the solution was degassed to prevent air bubbles inside the fibers. A high-resolution SE image of the phantom is shown in Figure 2(A). The fiber bundles consist of two fibers wrapped around a Plexiglas substrate shaped appropriately, hence the thin fibers on the left side of the cross. The volume fractions of the two crossing fiber bundles at their intersection are $v_1 = v_2 = 0.5$. A 2-D pulsed-gradient stimulated-echo sequence was used to obtain diffusion-weighted images of the phantom with the following experimental parameters: FOV= 2.5 cm $\times$ 2.5 cm, slice thickness = 1 cm, 16 $\times$ 16 Fourier points, TR/TE = 1500/14 ms, $\delta = 5$ ms, $\Delta = 250$ ms (to satisfy $\delta \ll \Delta$ and Eq. (1) as much as possible), eight diffusion gradient strengths $g = 0, 1, 2, 3, 3.5, 4, 4.5$, and 5 G cm^{-1} (i.e. $N_g = 7$ non-zero g values), $N_\theta = 30$ orientations according to the minimum energy spatial distribution obtained in [13]. A coarse resolution is used to emulate the temporal and spatial constraints for clinical imaging, cf. Figure 2(B). Thus, each pixel contains a bundle of fibers and the crossing of the fibers is not resolved. The QUAQ and MDTI reconstructions require 4 fitting parameters for single fibers $(D_\parallel, D_\perp, \theta_1, \psi_1)$, and 7 for two crossing fibers $(f_1, D_\parallel, D_\perp, \theta_1, \psi_1, \theta_2, \psi_2)$. For QUAQ, the series in Eq. (8) are truncated at $n = 3$ and $k = 6$.

The quality of the images was lessened by the fact that the PTFE produced a peak in the spectrum that encompassed the proton peak, which made shimming difficult. For the QUAQ and MDTI implementations, the results for which either $D_\parallel$ or $D_\perp$ are outside reasonable

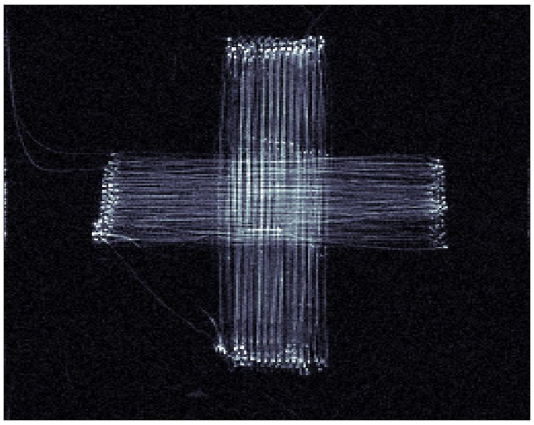

(A) SE image

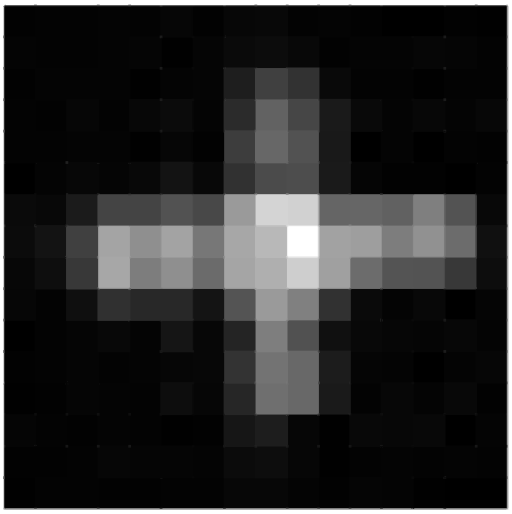

(B) Stimulated-echo image

Figure 2: MR images of the experimental phantom (FOV= 2.5 cm $\times$ 2.5 cm): (A) high-resolution SE image (256 $\times$ 256 resolution, TR/TE = 1000/10 ms); (B) low-resolution stimulated-echo image (16$\times$16 resolution, TR/TE = 1500/14 ms)

bounds ($> 2 \times 10^{-9}$ m^2 s^{-1}) are rejected. Moreover, the cases when $D_\parallel$ is found (significantly) smaller than $D_\perp$ using QUAQ are non-physical, and thus are also discarded. For both methods, these undesirable cases occur typically when the signal is too low and too noisy. However, with enough averaging (number of transient images $N_t = 6$ and 12), the results prove to be sufficiently useful to recover the geometry of the crossing fibers. Another source of error comes from the fact that the fiber size given by the manufacturer has a tolerance of $\pm 50\%$, resulting in erroneous estimation of the transverse diffusivity with QUAQ.

The results obtained by the QUAQ and MDTI algorithms using all the data collected ($N_t = 12$ averages,

ISSN: 1727-1983

$N_g = 7$ non-zero g values, and $N_\theta = 30$ orientations, i.e. 210 $\boldsymbol{q}$ values) are shown in Figures 3(A) and 3(B), respectively. For QUAQ, each pixel is represented as a cylinder of radius proportional to f_m and axis along (θ_m, ψ_m) in spherical coordinates, while for MDTI, we use an ellipsoid whose long and short axes are proportional to the products $(f_m D_\parallel)$ and $(f_m D_\perp)$, respectively, and whose long axis is oriented along (θ_m, ψ_m) in spherical coordinates ($m = 1$ when only one fiber is detected, and $m = 1$ or 2 when two are detected). Both methodologies recover the crossing of the fiber bundles well when comparing Figure 2(A) to Figures 3(A) and 3(B). For QUAQ, at the bottom and on the left of the crossing fiber bundles, a row of results have been discarded because of the noisy data there (cf. Figure 2(A)). The longitudinal diffusion coefficient matches that of water at the temperature inside the scanner ($\sim 11.5°$C), i.e. $D_\parallel \sim 1.6 \times 10^{-9}$ m^2 s^{-1}. For both methods, the signal-weighted volume fractions f_1 and f_2 do not quite match at the intersection due to the amount of noise in the non-diffusion-attenuated image (Figure 2(B)).

Discussion

The numerical and experimental results are promising and we set out to find out the influence of the sampling of $\boldsymbol{q}$-space (by varying N_g and N_θ), and the number of averages N_t ($= 6$ or 12). From the 30 orientations sampled in our experiments, we extracted the 15 orientations

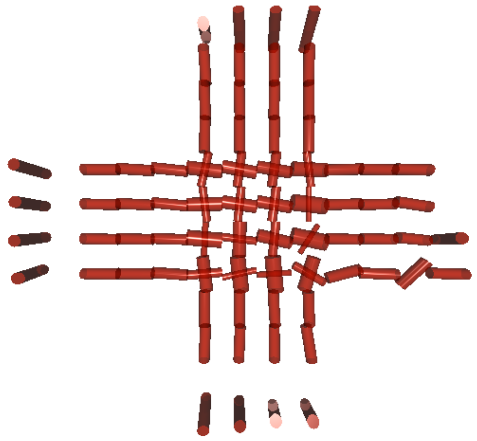

(A) QUAQ reconstruction

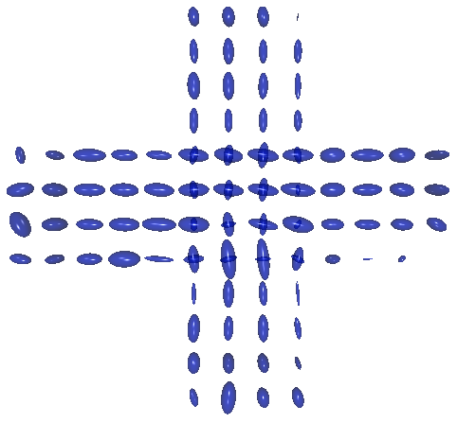

(B) MDTI reconstruction

Figure 3: Reconstruction of the phantom using all the experimental data available ($N_\mathrm{t} = 12$, $N_g = 7$, $N_\theta = 30$, i.e. 210 $\boldsymbol{q}$ values) with (A) QUAQ and (B) MDTI

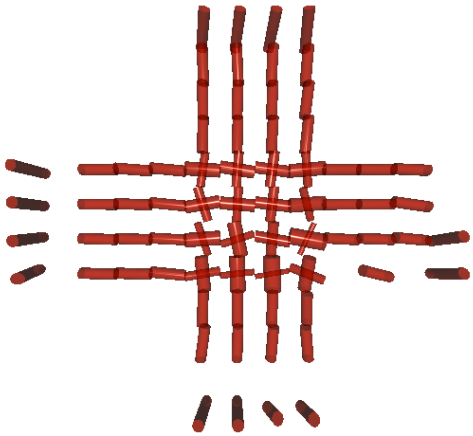

(A) QUAQ reconstruction

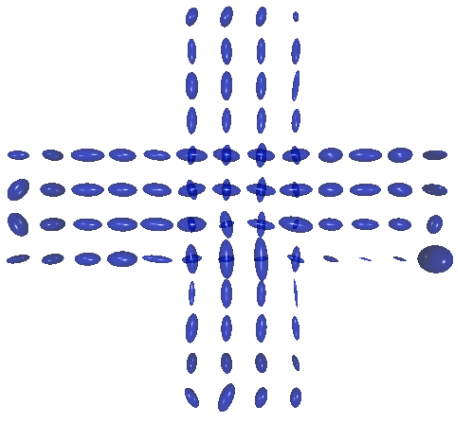

(B) MDTI reconstruction

Figure 4: Reconstruction of the phantom using partial experimental data ($N_\mathrm{t} = 6$, $N_g = 2$: $g = 4.5, 5$ G cm^{-1}, $N_\theta = 15$, i.e. 30 $\boldsymbol{q}$ values) with (A) QUAQ and (B) MDTI

ISSN: 1727-1983

that minimized the energy norm [13], so we could test our algorithm with $N_\theta = 15$ or 30. As shown in Figure 4, using less than 10% of the data collected ($N_\mathrm{t} = 6$, $N_g = 2$: $g = 4.5, 5$ G cm^{-1}, $N_\theta = 15$, i.e. 30 $\boldsymbol{q}$ values) yields reconstructions of the crossing fiber bundles using either QUAQ or MDTI that are similar to the ones shown in Figures 3(A) and 3(B). Only the data at the bottom row of the right arm of the cross is lost due to the lower SNR in that region, cf. Figure 2(A). We found out that, as illustrated in Figure 1, the data at large q values is more useful than the data at low values since the directionality is reflected in the high q regions. Therefore, if the data for the same amount of data ($N_\mathrm{t} = 6$, $N_g = 2$, $N_\theta = 15$, i.e. 30 $\boldsymbol{q}$ values) but with $g = 1$ and 5 G cm^{-1} is used, the reconstructions are not as good as with $g = 4.5$ and 5 G cm^{-1}. However, it must be kept in mind that the SNR drops as q increases.

In conclusion, the influence of the experimental parameters N_t, N_g, and N_θ are as follows. N_t is used to obtain a SNR sufficiently large to yield exploitable results. Both the number N_g and the distribution of q values are important. While $N_g > 1$ is necessary for QUAQ by construction, larger q (or g) values should be sampled to the limit that the SNR remains high enough. The number of orientations N_θ needs to be sufficiently large to determine the orientation of the fibers accurately, however since the variation of the normalized echo attenuation on a sphere at q constant is more pronounced for large q values, N_θ does not need to be excessively large provided data is collected for q large. We have shown here that a total of 31 $\boldsymbol{q}$ values are sufficient to recover the fiber bundle geometry, to be compared with 127 for HARDI [6], 253 for QBI [5], 496 used for CHARMED [4], and 515 used for DSI [3].

Conclusions

A quantitative approach (QUAQ) to extract information from $\boldsymbol{q}$-space MRI data is proposed and compared to a multi-modal DTI approach (MDTI). Numerical and experimental data are used to validate both approaches. In terms of retrieving the fiber orientations and crossings, both QUAQ and MDTI perform well even for relatively low SNR and a limited amount of data (31 images) compared to other methods [3–6]. However, in terms of physical parameters such as the diffusivities, QUAQ is shown to be more quantitative than MDTI. The next steps include testing on a biological sample and adding the presence of a hindered compartment following the CHARMED approach [4].

Acknowledgments

LGR and JGG are grateful to the NSF Sci. & Tech. Center (WaterCAMPWS, cooperative agreement CTS-0120978) and the Richard W. Kritzer Foundation for their financial support. DH and ZPL thank CRI, and the following grants: R01-CA098717, NSF-BES-0201876, and NIH-RR/EB03631-16. LC and BPS thank BIC for equipment usage.

References

[1] BASSER, P. J. and JONES, D. K. Diffusion-tensor MRI: theory, experimental design and data analysis - a technical review. *NMR Biomed.*, 15:456–467, 2002.

[2] BASSER, P. J., MATTIELLO, J., and LEBIHAN, D. Estimation of the Effective Self-Diffusion Tensor from the NMR Spin Echo. *J. Magn. Reson.*, Series B, 103:247–254, 1994.

[3] LIN, C. P., WEDEEN, V., CHEN, J., YAO, C., and TSENG, W. Validation of diffusion spectrum magnetic resonance imaging with manganese-enhanced rat optic tracts and ex vivo phantoms. *NeuroImage*, 19:482–495, 2003.

[4] ASSAF, Y., FREIDLIN, R. Z., ROHDE, G. K., and BASSER, P. J. New modeling and experimental framework to characterize hindered and restricted water diffusion in brain white matter. *Magn. Reson. in Med.*, 52:965–978, 2004.

[5] TUCH, D. S. Q-ball imaging. *Magn. Reson. in Med.*, 52:1358–1372, 2004.

[6] TUCH, D. S., REESE, T. G., WIEGELL, M. R., MAKRIS, N. G., BELLIVEAU, J. W., and WEDEEN, V. J. High angular resolution diffusion imaging reveals intravoxel white matter fiber heterogeneity. *Magn. Reson. in Med.*, 48:577–582, 2002.

[7] TANNER, J. and STEJSKAL, E. Restricted self-diffusion of protons in colloidal systems by the pulsed-gradient, spin-echo method. *J. Chem. Phys.*, 49(4):1768–1777, 1968.

[8] CALLAGHAN, P. T. Pulsed-gradient spin-echo NMR for planar, cylindrical, and spherical pores under conditions of wall relaxation. *J. Magn. Reson.*, Series A, 113:53–59, 1995.

[9] MARQUARDT, D. An algorithm for least-squares estimation of nonlinear paramters. *SIAM J. Appl. Math.*, 11:431–441, 1963.

[10] NEUMAN, C. H. Spin echo of spins diffusing in a bounded medium. *J. Chem. Phys.*, 60:4508–4511, 1974.

[11] GUDBJARTSSON, H. and PATZ, S. The Rician distribution of noisy MRI data. *Magn. Reson. in Med.*, 34:910–914, 1995.

[12] MILLS, R. Self-diffusion in normal and heavy water in the range 1-45°. *J. Phys. Chem.*, 77:685–688, 1973.

[13] HASAN, K. M., PARKER, D. L., and ALEXANDER, A. L. Comparison of gradient encoding schemes for diffusion-tensor MRI. *J. Magn. Reson. Imag.*, 13:769–780, 2001.

ISSN: 1727-1983